

# Preparation and characterization of porous alumina–zirconia composite ceramics

W. Pabst<sup>a,\*</sup>, E. Gregorová<sup>a</sup>, I. Sedlářová<sup>b</sup>, M. Černý<sup>c</sup>

<sup>a</sup> Department of Glass and Ceramics, Institute of Chemical Technology, Prague, Technická 5, 166 28 Prague 6, Czech Republic

<sup>b</sup> Department of Inorganic Technology, Institute of Chemical Technology, Prague, Technická 5, 166 28 Prague 6, Czech Republic

<sup>c</sup> Institute of Rock Structure and Mechanics, Academy of Sciences of the Czech Republic, V Holešovičkách 41, 182 09 Prague 8, Czech Republic

Available online 12 February 2011

## Abstract

Four types of porous alumina–zirconia composites on the alumina-rich side, differing in the zirconia content (10–40 wt.%), have been prepared by starch consolidation casting with different amounts of corn starch (10–50 vol.%), and the resulting microstructures have been studied via the Archimedes method, microscopic image analysis and mercury porosimetry (bulk density, porosity, pore size and pore size distribution), with special regard to the evolution of the microstructure as a result of (partial) sintering in the temperature range 1100–1530 °C. An influence of the composition on pore size and shape has been observed. Elastic properties (Young's moduli) of the composites are measured via the impulse excitation method and the resonant frequency method and compared with micromechanical relations expressing the dependence of Young's modulus on porosity. It is found that the exponential relation and the sigmoidal average provide the best descriptions for the Young's moduli of materials with this type of microstructure.

© 2011 Elsevier Ltd. All rights reserved.

**Keywords:** A. Sintering; A. Slip casting; B. Composites; B. Microstructure-final; B. Porosity; C. Mechanical properties; D. Al<sub>2</sub>O<sub>3</sub>; ZrO<sub>2</sub>; Pore size; Elastic modulus

## 1. Introduction

Alumina–zirconia composite ceramics with compositions on the alumina-rich side, so-called ZTA (zirconia-toughened alumina) ceramics, are widely used materials for diverse structural applications, mainly because of their relatively high fracture toughness.<sup>1–3</sup> The majority of these applications to date is based on dense, fully sintered materials without porosity. It is challenging, however, to use ZTA compositions also for the preparation of porous ceramics and thus to combine their generally favorable mechanical properties with the functionality of porous materials (light weight, low thermal conductivity, low elastic modulus and, possibly, fluid permeability).<sup>4–6</sup> We would like to emphasize that the acronym “ZTA” and its counterpart “ATZ”, is often used simply as a shorthand notation for alumina–zirconia composite ceramics with compositions on the alumina-rich and zirconia-rich side, without direct reference to the toughening effect. In

the case of ZTA – as here – this is justifiable, because a toughening effect may be expected, in contrast to ATZ, for which one may at best propose the reinterpretation of this acronym as “alumina-containing tetragonal zirconia”.

A popular method for preparing porous ceramics is the use of pore-forming agents that burn out during the firing step. One of the most frequently used pore-forming agents is starch.<sup>7–22</sup> Starches have several advantages (hygiene, ecology, economy, quality, size range), but most important from the engineering point of view is the residual-free burnout due to the negligible ash content.<sup>23</sup> As is well known, starches can be used as mere pore-forming agents by simply adding them e.g. to slurries for traditional slip-casting or as combined pore-forming and body-forming agents (stiffening or consolidating agents) in starch consolidation casting.<sup>24–34</sup> The principles of both processes have been described in many papers.<sup>18–34</sup> Porous ceramics of porosities up to approx. 50% are readily achieved by both methods, but the preparation of ceramics with porosity higher than 50% by these two methods alone is difficult and has not been very successful. One possibility to achieve higher porosities is to combine these methods with partial sintering. The resulting materials

\* Corresponding author.

E-mail addresses: [pabstw@vscht.cz](mailto:pabstw@vscht.cz), [Willi.Pabst@vscht.cz](mailto:Willi.Pabst@vscht.cz) (W. Pabst).

will exhibit hierarchical microstructures with strongly bimodal pore size distributions: large pores as remnants of the burnt-out pore-forming agents and small interstitial pores between the ceramic powder grains. The large pores are essentially convex cavities which may be in contact or interconnected when the content of pore-forming agent (starch) is higher. Their shape corresponds more or less to that of the original pore-forming agents (more for traditional slip casting, less for starch consolidation casting, due to the interfering swelling step). On the other hand, the small interstitial pores are concave and form a continuous (i.e. completely open) pore space until sintering proceeds to a degree sufficient for pore closure.<sup>35,36</sup> In this paper the method of starch consolidation casting has been combined with partial sintering to achieve porosities significantly higher than 50%.

With respect to the actual and potential applications of porous ceramics these materials require complex microstructural characterization. That means, except for bulk density and open porosity (which are accessible directly via Archimedes measurements), at least the total porosity and the pore size should be characterized. The total porosity can be calculated from bulk density when the theoretical density is known. This method is usually more reliable than the alternative method of determining the (total) porosity via image analysis from cuts or polished sections by invoking the Delesse–Rosin law (i.e. the rule that “area fraction of pore sections” = “volume fraction of pores” under the assumptions of isotropy, uniformity and randomness<sup>37–39</sup>), because sample preparation is much easier and imaging artifacts are of no concern. Pore size is a bigger problem: apart from the fact that the pore size must always be given in terms of either equivalent or statistical values (diameters), the concept of pore size itself requires the pores to be well-defined, isolated objects, preferentially with a convex shape, in a matrix. Only in this case a 2D pore section equivalent area diameter distribution can be measured via single-object-based image analysis and subsequently transformed into a true 3D pore equivalent diameter distribution, e.g. using a Saltykov transformation<sup>37</sup> (when the pore shape is not too far from isotropic). In other words, in order to determine an unambiguous pore size distribution from image analysis (or tomography, for that matter) the microstructure, if isotropic, must be of the matrix-inclusion type. This is not always the case. For example, partially sintered microstructures usually have a connected pore space. That means they are bicontinuous, with both the solid phase (skeleton) and the pore space forming connected paths from one side to the other side of a macroscopic body. Therefore microscopic image analysis can be used to determine an unambiguous pore size distribution only in exceptional cases. Nevertheless, an average measure of pore size can be determined by image analysis (or tomography) even if the pores are not well-defined, isolated objects: the mean intercept diameter (mean chord length).<sup>37–39</sup> This is a robust statistical size measure in the sense that it remains well-defined even if the microstructure is bicontinuous, with a completely interconnected pore space (consisting of convex, concave and saddle surfaces, but without any single pores). Note, however, that the mean pore size determined by this method always depends on the resolution of the microscopic method used, which is of order 1  $\mu\text{m}$  when light-

optical microscopy is used. It should also be emphasized that the mean intercept technique yields an arithmetic average of a number-weighted distribution. That means, when applied in an unbiased way to a microstructure with a wide pore size distribution, the calculated mean intercept should not be expected to correspond to an allegedly evident “average pore size” based on mere visual inspection. If a pore size distribution is required, mercury porosimetry is of course the traditional method of choice. It has the advantage of covering a fairly wide size range (from tens of  $\mu\text{m}$  in a low-pressure equipment) down to the nanometer range in high-pressure equipment.<sup>40</sup> One has to be aware of the fact, however, that mercury porosimetry is based on the intrusion of mercury into the pore space and thus only open pores are probed. Moreover the equivalent diameters determined via mercury porosimetry are size measures based on the Washburn equation, i.e. obtained assuming a porous medium with straight, constant-diameter, non-intersecting cylinder pores.<sup>40</sup> That means, in the case of large pore cavities (cells) connected by small pore channels or throats (window cells) mercury porosity yields a (equivalent) pore throat diameter distribution, while image analysis (and tomography) would yield a (equivalent) pore cavity diameter distribution. In this paper the Archimedes method, image analysis (mean intercept method) and mercury porosimetry are used to characterize the microstructure of the porous ZTA ceramics prepared.

The toughening effect of zirconia grains in a (dense) alumina matrix has been well investigated during the last few decades now<sup>1–3</sup> and remarkable properties, mainly with respect to strength and fracture toughness have been achieved in these materials.<sup>1–3</sup> Concerning elastic constants, in particular Young’s moduli, it is quite easy to predict their effective values for dense composites of arbitrary composition, because the “phase contrast” of the end members (ratio of the Young’s moduli of alumina, 400 GPa, and zirconia, 205 GPa) is only approx. 2:1 and therefore the upper and lower Hashin–Shtrikman bounds, which can be invoked to estimate the effective moduli of isotropic materials,<sup>41,42</sup> are close enough to yield a very precise theoretical prediction, which has been confirmed experimentally several times.<sup>41,42</sup> The situation is completely different for porous materials.<sup>43–54</sup> Although the elastic modulus of the matrix can be reliably predicted when the composition is known, it has been believed until recently that such a prediction is not possible in the case of porous materials. From a strictly mathematical point of view this is of course true: there is no universal relation for the prediction of effective properties of porous materials, simply because a unique porosity dependence does not exist. Nevertheless, research in the last few years has indicated that certain types of porosity dependences are evidently “preferred by nature”. Among these are the exponential relation proposed by Pabst and Gregorová<sup>41,46–49</sup> and the sigmoidal average proposed by Pabst et al.<sup>50,51</sup> The theoretical derivation of the first is based on the functional equation approach (a kind of effective medium approximation) described in Ref.<sup>44</sup>, while the latter is a purely empirical relation, based on a weighted average of upper and lower bounds.<sup>51</sup> The sigmoidal average seems to be the simplest type of average that is generalizable to composites of arbitrary phase contrast by taking into account the upper and

lower bound and at the same time usable for composites with infinite phase contrast, i.e. porous media. On the other hand, all experimental findings to date indicate that our exponential relation is appropriate for predicting the porosity dependence of the thermal conductivity, Young's modulus and other effective properties of porous materials prepared with pore-forming agents. The adequacy of both relations for estimating the porosity dependence of properties such as thermal conductivity and Young's modulus has been demonstrated in several experimental papers,<sup>21,22,52,53</sup> but only up to porosities of approx. 50%. In this paper first evidence is given of the fact that both relations provide the best *a priori* estimates currently available even for higher porosities, viz. up to approx. 70%. The Young's moduli for this paper were measured by the resonant frequency technique and the impulse excitation technique in order to double-check the results.

## 2. Experimental

For the preparation of porous ZTA ceramics by starch consolidation casting commercial alumina ( $\alpha$ -Al<sub>2</sub>O<sub>3</sub>) and zirconia (t-ZrO<sub>2</sub> with 3 mol.% Y<sub>2</sub>O<sub>3</sub>) powders with submicron particle size have been used in this work: AA04 (Sumitomo, Japan; median particle size approx. 0.4  $\mu$ m, specific surface area approx. 4 m<sup>2</sup>/g) and TZ-3Y (Tosoh, Japan; median particle size approx. 0.4  $\mu$ m, crystallite size 28–40 nm, specific surface area approx. 16 m<sup>2</sup>/g). Corn starch (Gustin, Dr Oetker, Czech Republic) with a median diameter of 14  $\mu$ m has been used as the pore- and body-forming agent. Aqueous suspensions containing the ceramic powder mix, corn starch and deflocculant (Dolapix CE64, Zschimmer & Schwarz, Germany) in a concentration of 1 wt.% (related to the ceramic powder) were prepared by homogenization in polyethylene bottles with alumina balls on a laboratory shaker (HS260, IKA, Germany) for 2 h and by ultrasonication (UP200S, Dr Hielscher, Germany). Four basic types of composite ceramics were prepared, containing 10, 20, 30 and 40 wt.% of zirconia (labelled A90Z10, A80Z20, A70Z30 and A60Z40). Of each of these four ZTA compositions four variants with different porosities made from suspensions with nominal (i.e. related to the ceramic powder) starch contents in the range 10–50 vol.% were prepared (taking the density of dry corn starch as 1.5 g/cm<sup>3</sup>). The concentrations of ceramic powders in the suspensions were 73–75 wt.% (lower for larger starch contents and vice versa). The as-prepared, ready-to-cast mixed slurries were cast into brass molds with a cylindrical cavity of internal diameter 7 mm and length 70 mm; before casting the mold surfaces were coated with an alkali-free grease (Apeizon M Grease, Apeizon, UK) for easy demolding. The molds with the slurries were heated to 80 °C for 2.5 h. After consolidation of the starch-containing slurries, the molds were cooled to room temperature, the samples taken out and dried under ambient conditions for 24 h, and then at 60, 80 and 105 °C until mass constancy, with a 2 h dwell at the first two temperatures. The as-dried samples were fired at 1100, 1200, 1300 and 1400 °C (partial sintering of the matrix) or 1530 °C (full sintering of the matrix) with a heating rate of 2 °C/min and a 2 h dwell. The sintering temperature of 1530 °C has been chosen based on previous work in

which it has been demonstrated that theoretical densities higher than 99% can be achieved for the ZTA composites of this work prepared by slip casting into plaster molds.<sup>54</sup>

XRD investigations of samples after firing have been performed with a Siemens D5005 powder diffractometer (Siemens, Germany) in Bragg-Brentano geometry using CuK $\alpha$  radiation (divergence slit 1°, 40 kV, 40 mA, step size 0.05° in 5 s) and quantitative phase analysis has been made using two types of Rietveld-based software packages (Siroquant/Sietronics, Australia and Topas/Bruker, Germany). SEM micrographs have been obtained with a Leo 1450 VP (Carl Zeiss Jena, Germany). The as-fired samples were characterized with respect to shrinkage by a slide caliper. Their bulk density and open porosity were determined via the Archimedes technique after boiling in water. The total porosity was determined based on the theoretical density of each composition, taking the density values 4.0 g/cm<sup>3</sup> and 6.1 g/cm<sup>3</sup> for the end members alumina and zirconia, respectively. Polished sections were prepared from the samples with fully sintered matrix (fired at 1530 °C) and pore size distributions were measured via the mean intercept technique<sup>37–39</sup> using commercial image analysis software (Lucia G, Laboratory Imaging, Czech Republic) on optical micrographs (Jenapol, Zeiss, Germany). More than 1000 objects have been measured for each sample by superimposing a square grid on the micrograph and dividing the integral chord length inside pore sections by the number of intersections (=half the number of intersection points with the pore perimeter). Mercury porosimetry (AutoPore IV 9500, Micromeritics, USA) was used to determine the pore size distribution (more precisely the pore throat size distribution) and the apparent density (i.e. the density including closed pores) of all types of samples. In the case of partially sintered sample this technique reveals not only the interconnecting throats between the large pores but also the very small interstitial pores between the ceramic grains.

The Young's moduli of all composites were measured by the resonant frequency technique and the impulse excitation technique via two signal types, using two different types of equipment: firstly via longitudinal vibrations using electromechanical excitation (Erudite, CNS Electronics, UK) and an oscilloscope to find resonant frequencies, and secondly via flexural vibrations using an impulse excitation instrument (RFDA 23, IMCE, Belgium) with fast Fourier transformation software. In the case of longitudinal vibrations (resonant frequency technique) the Young's moduli were calculated according to the approximate formula

$$E = \rho(2f_1L)^2, \quad (1)$$

an approximation valid for slender cylindrical specimen,<sup>55</sup> where  $\rho$  is the bulk density,  $f_1$  the fundamental resonant frequency for longitudinal vibrations and  $L$  the specimen length. In the case of flexural vibrations (impulse excitation technique) the Young's moduli were calculated via the RFDA-MF software (according to ASTM C 1259) via the equation

$$E = 1.6067 \left( \frac{L^3}{D^4} \right) (m \cdot f_f^2) C, \quad (2)$$

where  $D$  is the diameter of the rod,  $m$  the mass of the rod,  $f_f$  the fundamental resonant frequency for flexural vibrations and  $C$  a correction factor dependent on the aspect ratio of the rod and the Poisson ratio of the material,<sup>56</sup> see also Ref.<sup>57</sup>.

### 3. Results and discussion

Figs. 1 and 2 show the microstructural characteristics (bulk density, open and total porosity) and shrinkage (after firing) of porous alumina–zirconia composites with 10, 20, 30 and 40 wt.% zirconia (A90Z10, A80Z20, A70Z30, A60Z40) prepared from suspensions with starch contents in the range 10–50 vol.% after sintering at 1530 °C.

From these values it is evident that the total porosity is a sensitive function of the starch content in the suspension, but is substantially independent of the alumina–zirconia ratio in the composites. However, due to the swelling of starch, which is typical for the starch consolidation process,<sup>30</sup> the porosity in the ceramic after firing does not correspond directly to the nominal starch content in the suspension. For example, for 10 vol.% of corn starch in the suspension (related to ceramics) the resulting porosity after firing is not 10% but 26–28% (23–25% is open porosity). On the other hand, when the starch content in

the suspension is sufficiently high, swelling is not completely free, but constrained by steric effects (excluded volume effects). Therefore with a starch content of 50 vol.% in the suspension it is possible to achieve total porosities of 50–51% (essentially all open). All these findings are in complete agreement with previous findings for alumina ceramics<sup>18,32</sup> and other starch types.<sup>19,20</sup> Of course, the bulk densities (for comparable porosities) exhibit an increasing trend with increasing zirconia content. Shrinkage after firing seems to be independent of the starch content in the suspension (or the resulting starch-induced porosity). It is in the overall range 17–22%, tending to the lower value for the low-zirconia composites A90Z10 and A80Z20 and to the higher ones for the high-zirconia composites A70Z30 and A60Z40. The independence of shrinkage on the starch content is an indication of the fact that it is essentially the shrinkage of the matrix (we recall that it is well known that large pores in a fine-grained matrix do not by themselves significantly contribute to shrinkage<sup>35,36</sup>). The latter trend (slight dependence on the zirconia content) is a consequence of the fact that the matrix shrinkage during sintering depends on the packing fraction of the green bodies,<sup>58</sup> which is usually lower for zirconia (and ZrO<sub>2</sub>-rich composites) than for alumina (and Al<sub>2</sub>O<sub>3</sub>-rich composites).

XRD phase analysis indicates that the monoclinic/tetragonal ratio is below 0.20 in all ZTA composites prepared in this work (5–13% and 8–20% for composites fired at 1100 and 1530 °C, respectively), without a recognizable correlation to the overall zirconia content in the composite. It must be emphasized, however, that the absolute contents of monoclinic ZrO<sub>2</sub> in the alumina–zirconia composites are much lower, viz. 0.6–7%, so that the error in the total porosity computation becomes in fact negligibly small.

Figs. 3 and 4 show the microstructural characteristics (bulk density, open and total porosity) and shrinkage (after firing) of porous alumina–zirconia composites with 10, 20, 30 and 40 wt.% zirconia (A90Z10, A80Z20, A70Z30, A60Z40) prepared from suspensions with 50 vol.% corn starch after partial sintering to different temperatures (1100, 1200, 1300 and 1400 °C) and after full matrix sintering at 1530 °C.

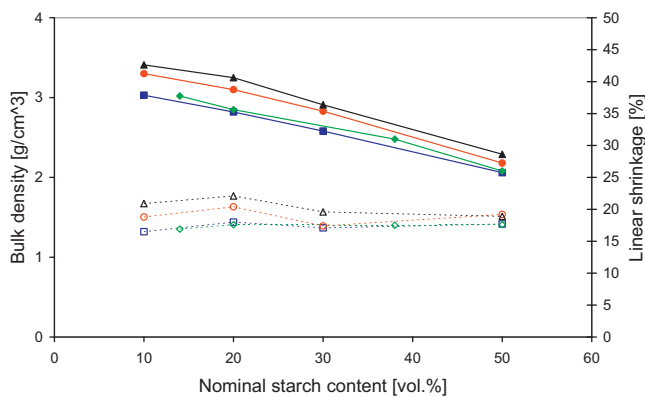


Fig. 1. Dependence of the bulk density (full symbols, left ordinate) and the linear shrinkage (empty symbols, right ordinate) after firing on the nominal starch content (triangles A60Z40, circles A70Z30, diamonds A80Z20, squares A90Z10).

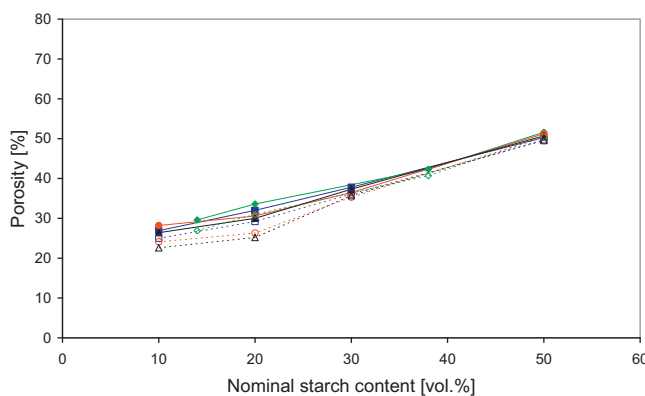


Fig. 2. Dependence of the total porosity (full symbols) and the open porosity (empty symbols) after firing on the nominal starch content (triangles A60Z40, circles A70Z30, diamonds A80Z20, squares A90Z10).

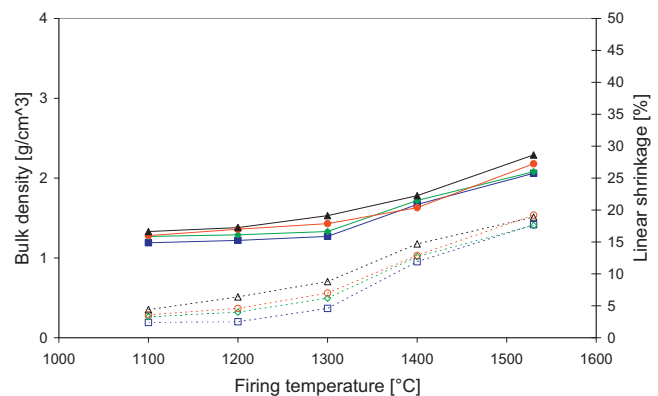


Fig. 3. Dependence of the bulk density (full symbols, left ordinate) and the linear shrinkage (empty symbols, right ordinate) on the firing temperature (triangles A60Z40, circles A70Z30, diamonds A80Z20, squares A90Z10).

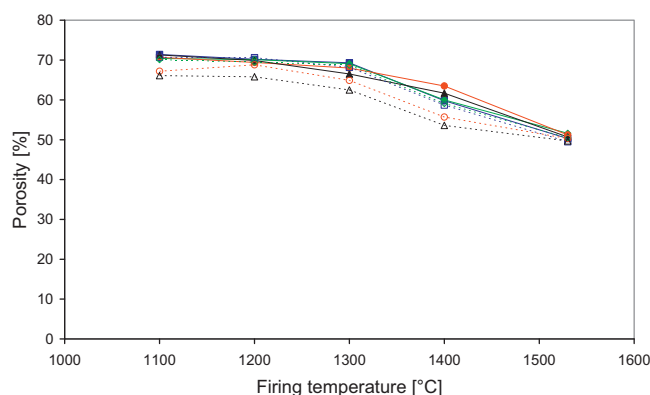


Fig. 4. Dependence of the total porosity (full symbols) and the open porosity (empty symbols) on the firing temperature (triangles A60Z40, circles A70Z30, diamonds A80Z20, squares A90Z10).

The most important finding is that porosities up to 70–71% can be achieved when use of the pore-forming agent (corn starch) is combined with partial sintering, whereas without partial sintering porosities significantly higher than 50% cannot be achieved without risking collapse of the structure, resulting in serious deformation of the green bodies.<sup>32</sup> As expected, the bulk density increases with firing temperature (from 1.2 to 1.3 g/cm<sup>3</sup> after firing at 1100 °C to 1.6–1.8 g/cm<sup>3</sup> after firing at 1400 °C and 2.1–2.3 g/cm<sup>3</sup> after firing at 1530 °C), and the shrinkage increases accordingly (from 2–4% after firing at 1100 °C to 12–15% after firing at 1400 °C and to 18–19% after firing at 1530 °C), but both characteristics depend only very slightly on the zirconia content. With increasing firing temperature the porosities decrease from the aforementioned values of 70–71% after firing at 1100 °C to 60–64% after firing at 1400 °C and to 50–51% after firing at 1530 °C (total porosity values). As far as total porosities are concerned, differences between the composites are insignificant. However, there seems to be a small, but statistically significant, effect concerning open porosity. For the alumina–zirconia composites with low zirconia content (A90Z10 and A80Z20) the latter is in all cases less than 1.1% (in absolute percentage) below the total porosity value, whereas for the composites with high zirconia content (A70Z30 and A60Z40) they are up to 7.8% below the total porosity values, i.e. there is a certain amount of closed porosity, increasing with higher firing temperature (from 0.6–5.2% after firing at 1100–1200 °C to 3.1–7.8% after firing at 1300–1400 °C). The fact that the closed pore content is increasing with increasing firing temperature can be explained in terms of the classical pore closure concept at the final stage of sintering,<sup>35,36</sup> i.e. a transition from an open network of concave interstitial pores – modelable e.g. by interconnected cylindrical channels according to the Coble model<sup>35,36</sup> – to closed, i.e. isolated, convex pores. This effect is more important in zirconia-rich composites because the zirconia powder used here is known to have a slightly lower sintering temperature than the alumina powder used. This behavior can be considered as typical for common alumina–zirconia composites where the alumina and zirconia grain size is not dramatically different.

Figs. 5 and 6 show micrographs of polished sections of porous alumina–zirconia composites after firing at 1530 °C. Fig. 5 shows the microstructures of different compositions (from A90Z10 to A60Z40) prepared with 10 vol.% of corn starch. The microstructures are similar, but it is interesting that for the zirconia-rich compositions, especially A60Z40, the pore shape is more irregular and often non-convex (locally concave). This finding confirms several previous observations in our laboratory and seems to be typical for zirconia and zirconia-rich composites. The mean pore sizes listed in Table 1, which have been determined via the mean intercept method, confirm a decrease in the measured pore size from low-zirconia to high-zirconia composites (e.g. for composites prepared from suspensions with 10 vol.% starch the mean intercepts decrease from 16.5 to 11.5 μm when going from A90Z10 to A60Z40). Fig. 6 shows the microstructures of alumina–zirconia composites with low zirconia content (A90Z10) prepared from suspensions with different starch contents (10, 20, 30 and 50 vol.%). It is evident that pore size in the fired ceramics decreases significantly with increasing starch content in the suspensions. Also this trend is quantitatively confirmed by the values in Table 1 (e.g. for A90Z10 composites the mean intercepts decrease from 16.5 to 12.0 μm when going from to samples prepared from suspensions with 10–50 vol.% of corn starch). It has to be noted that the mean intercept technique does not allow to distinguish between single pores and apparent pore “agglomerates” (which may result from pore wall breaking, a frequent and usually unavoidable artifact of sample preparation); therefore, since “pore overlap” is more of a problem in highly porous ceramics, the pore size differences determined by this method for samples prepared with different starch contents are always underestimated. We would also like to recall the well-known fact that the fact that pores appear isolated in a 2D cut (polished section) does not allow any conclusions about pore closure in 3D. We emphasize that the porosity of ceramics prepared by starch consolidation casting is always essentially open and interconnected (cf. the total and open porosity values in Fig. 2), although the micrographs might give the wrong impression that for ceramics prepared with low starch contents there is a significant amount of closed porosity. In ceramics prepared by starch consolidation casting there is no percolation threshold as for ceramics prepared by simple slip-casting with pore-forming agents,<sup>18</sup> because with starch contents that would possibly lead to porosities below the percolation threshold it is not possible to achieve rigid green bodies.

Table 1

Pore size of porous alumina–zirconia ceramics of different composition after firing at 1530 °C, determined by image analysis of polished sections (mean intercepts).

Sample type	Pore size [μm]			
	10 vol.% starch	20 vol.% starch	30 vol.% starch	50 vol.% starch
A90Z10	16.5	13.5	12.9	12.0
A80Z20	14.7	13.4	11.6	11.5
A70Z30	13.4	10.7	10.4	10.7
A60Z40	11.6	11.7	10.0	9.5

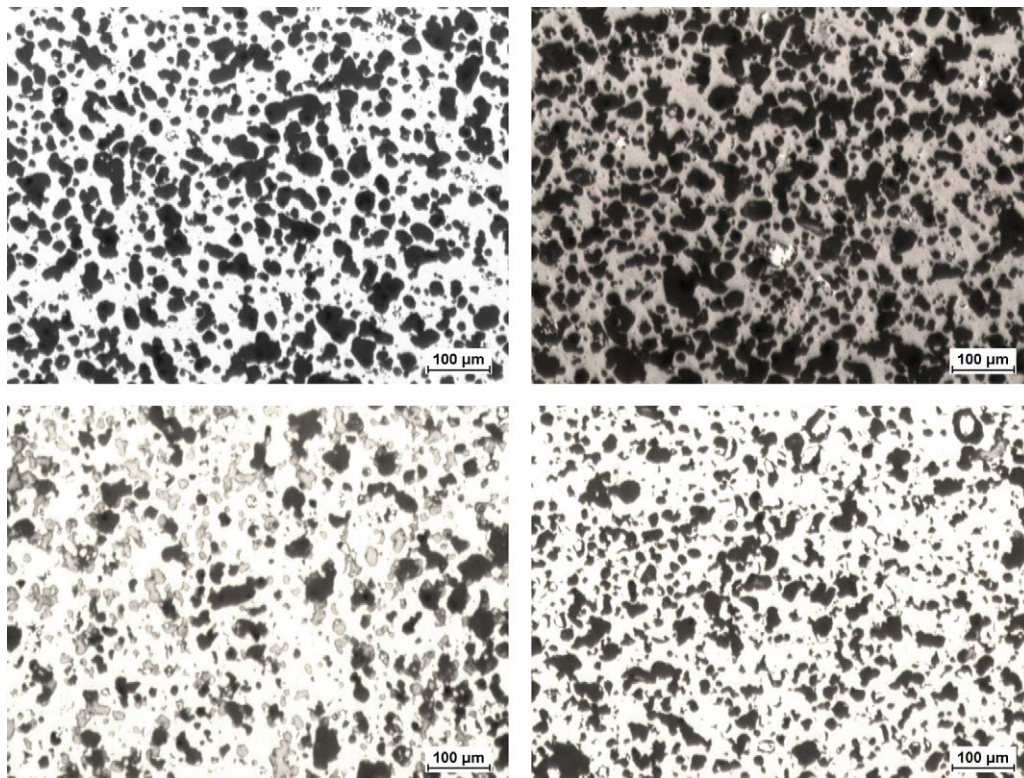


Fig. 5. Micrographs of polished sections of porous alumina–zirconia composites prepared with 10 vol.% of corn starch after firing at 1530 °C (left top – A90Z10, right top – A80Z20, left bottom – A70Z30, right bottom – A60Z40).

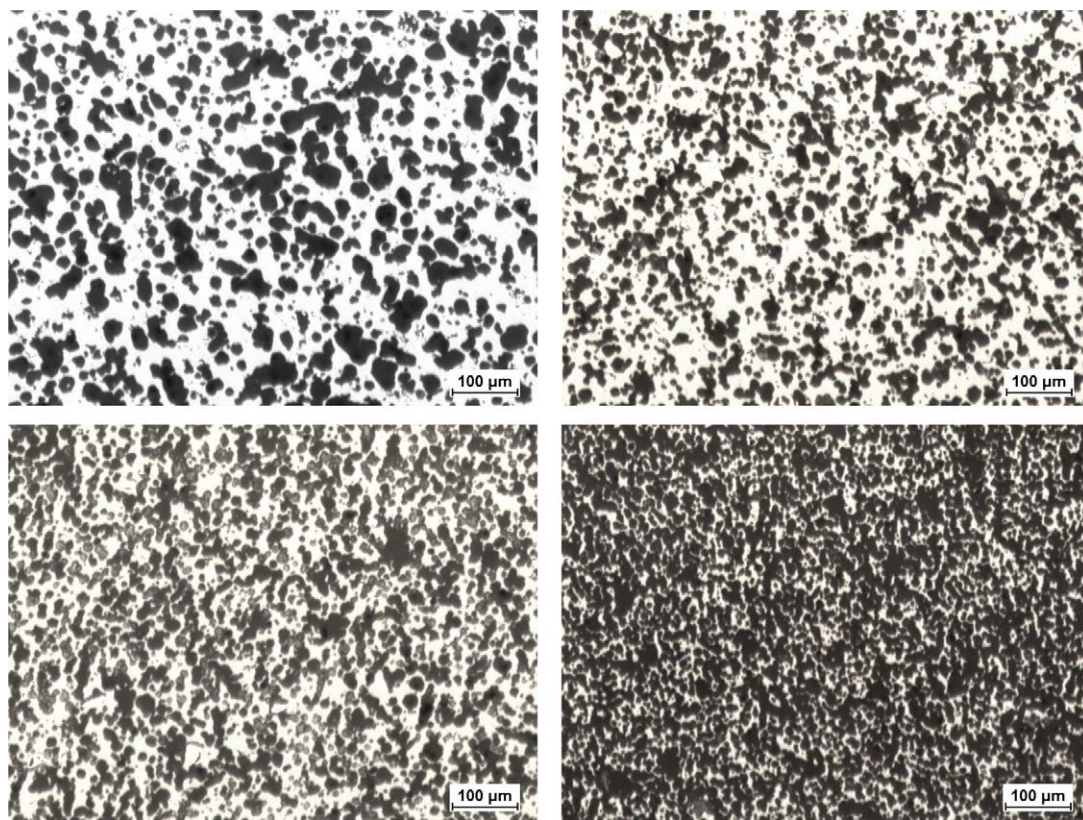


Fig. 6. Micrographs of polished sections of porous alumina–zirconia composites A90Z10 prepared with different nominal contents of corn starch after firing at 1530 °C (left top – 10 vol.%, right top – 20 vol.%, left bottom – 30 vol.%, right bottom – 50 vol.%).

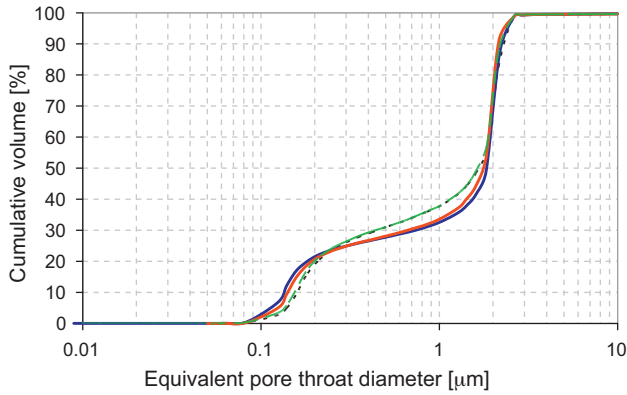


Fig. 7. Pore size distributions (cumulative curves) measured via mercury porosimetry for porous alumina–zirconia composites of different composition prepared with 50 vol.% of starch after partial sintering at 1200 °C (dotted curve – A90Z10, dashed curve – A80Z20, right curves – A60Z40 and A70Z30).

Figs. 7 and 8 show the results of mercury porosimetry (cumulative and frequency curves) for alumina–zirconia composites of different composition (from A90Z10 to A60Z40) prepared with 50 vol.% of corn starch after firing at 1200 °C. The distribution measured by mercury porosimetry is bimodal due to the pore cavity size resulting from starch burnout, which can only be determined by image analysis and is in the range 10–17 μm, cf. Table 1, corresponding to the median diameter of the starch granules (approx. 14 μm<sup>17</sup>). The median values of the pore throat diameter distributions are 1.6–1.8 μm, while the mode values are 1.8 μm and 0.1–0.2 μm, i.e. 100–200 nm for the pore throats and interstitial pore openings, respectively. It is evident that there is no significant difference between the composite types, i.e. the microstructure achieved is a result only of processing, i.e. the microstructure achieved is essentially independent of the material. Figs. 9 and 10 show SEM micrographs of the fracture surfaces of A60Z40 samples after partial sintering at 1100 °C. In Fig. 9 the large pores (with a size of order 10 μm) are interconnected by pore openings (cell windows, a few μm in diameter), and in Fig. 10 partially sintered submicron-sized particles are visible, between which there are small interstitial pores with a size of order 100 nm.

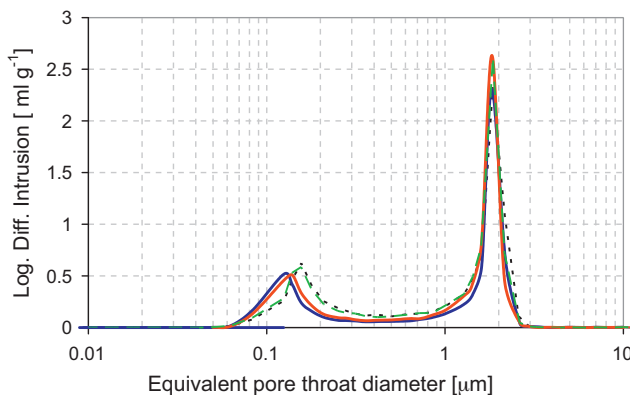


Fig. 8. Frequency curves corresponding to Fig. 7.

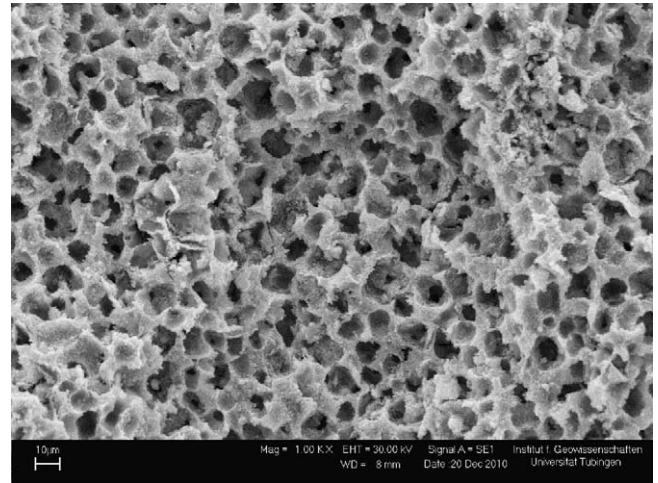


Fig. 9. SEM micrograph of A60Z40 prepared with 50 vol.% of corn starch after firing at 1100 °C (magnification 1000×).

Figs. 11 and 12 show the results of mercury porosimetry (cumulative and frequency curves) for alumina–zirconia composites of different composition (again from A90Z10 to A60Z40) prepared with 50 vol.% of corn starch after firing at 1530 °C. It is evident that the smallest interstitial pores have vanished, indicating that the matrix is densely sintered now (this conclusion is also confirmed by calculating the so-called apparent density, i.e. the density with closed but without open pores: the resulting values are within 98–99% of the theoretical density of the materials). The pore throat diameters are in the range 1.4–2.2 μm (median values similar to the range mentioned above), again without any recognizable dependence on the material. Figs. 13 and 14 show the dependence of the microstructure on the firing temperature for the composite A60Z40. It is nicely seen how the cumulative volume of the small interstitial pores gradually decreases with increasing firing temperature, and finally the largest pores (pore throats) suffer a jumpwise increase in size, indicating that small interstitial pores

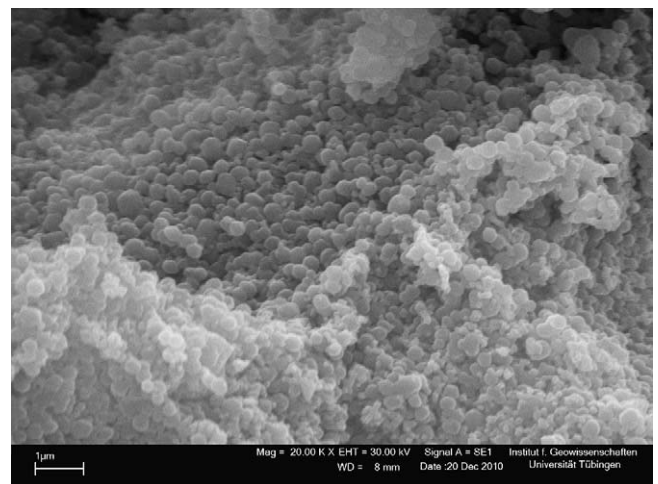


Fig. 10. SEM micrograph of A60Z40 prepared with 50 vol.% of corn starch after firing at 1100 °C (magnification 20,000×).

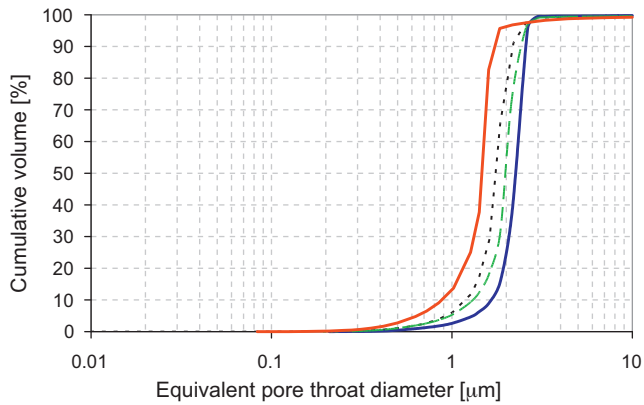


Fig. 11. Pore size distributions (cumulative curves) measured via mercury porosimetry for porous alumina–zirconia composites of different composition prepared with 50 vol.% of starch after firing at 1530 °C (left curve – A70Z30, dotted curve – A90Z10, dashed curve – A80Z20, right curve – A60Z40).

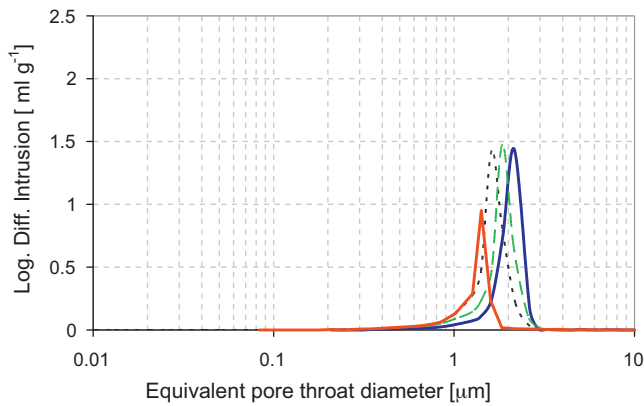


Fig. 12. Frequency curves corresponding to Fig. 11.

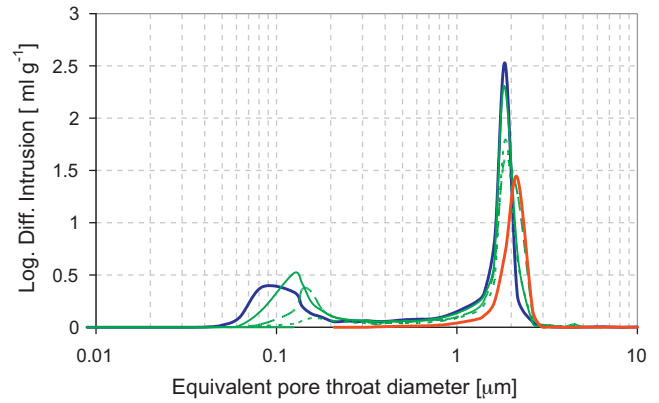


Fig. 14. Frequency curves corresponding to Fig. 13.

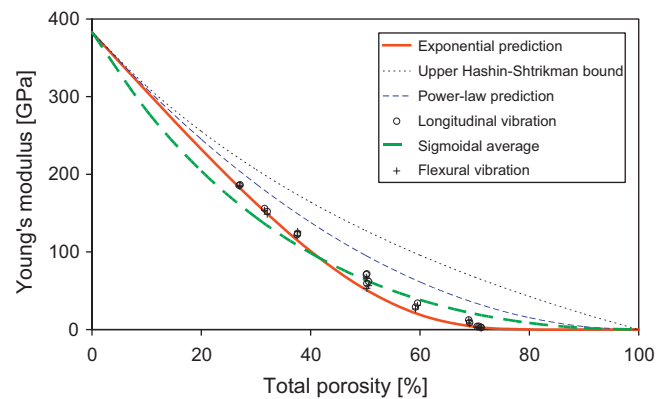


Fig. 15. Young's moduli of alumina–zirconia composites A90Z10 measured via the resonant frequency technique (circles) and the impulse excitation technique (pluses) and comparison with four admissible predictions (thin dotted – upper Hashin Shtrikman bound, thin dashed – power-law prediction, thick full – exponential prediction, thick dashed – sigmoidal average).

have migrated to the large cavities in the final stage of matrix sintering.

Figs. 15–18 show the dependence of the Young's modulus on the total porosity for alumina–zirconia composites of different composition (from A90Z10 to A60Z40) prepared with

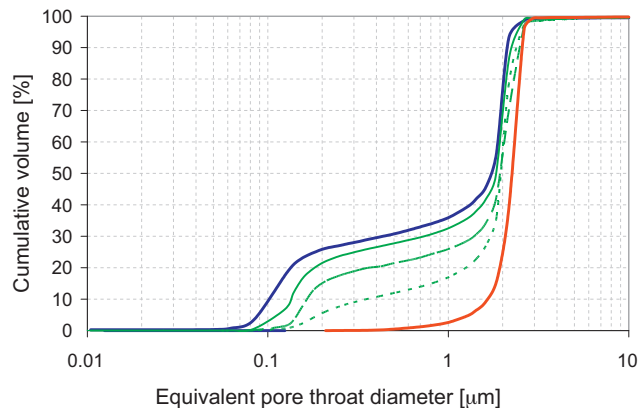


Fig. 13. Pore size distributions (cumulative curves) measured via mercury porosimetry for porous alumina–zirconia composites of composition A60Z40 prepared with 50 vol.% of starch after firing at 1100 °C, 1200 °C, 1300 °C, 1400 °C and 1530 °C (from left to right, respectively).

different starch contents (in the range 10–50 vol.%, related to the ceramic powders) after firing to different temperatures ranging from 1100 °C to 1530 °C. In these figures the measured val-

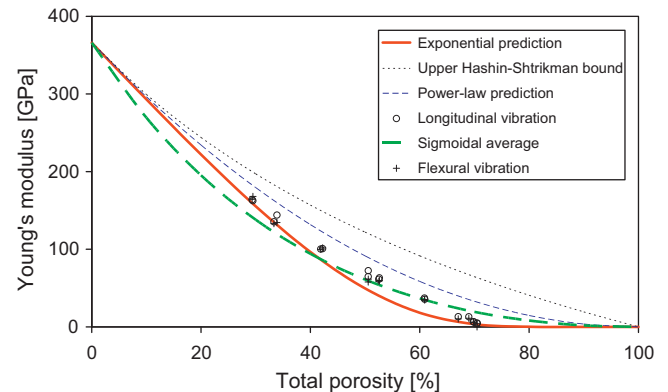


Fig. 16. Young's moduli of alumina–zirconia composites A80Z20 measured via the resonant frequency technique (circles) and the impulse excitation technique (pluses) and comparison with four admissible predictions (thin dotted – upper Hashin Shtrikman bound, thin dashed – power-law prediction, thick full – exponential prediction, thick dashed – sigmoidal average).

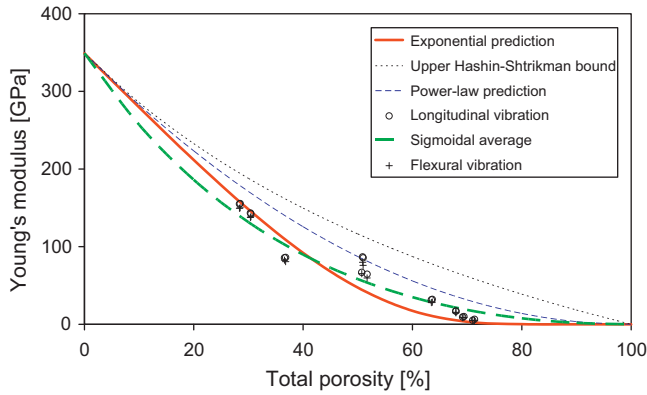


Fig. 17. Young's moduli of alumina–zirconia composites A70Z30 measured via the resonant frequency technique (circles) and the impulse excitation technique (pluses) and comparison with four admissible predictions (thin dotted – upper Hashin Shtrikman bound, thin dashed – power-law prediction, thick full – exponential prediction, thick dashed – sigmoidal average).

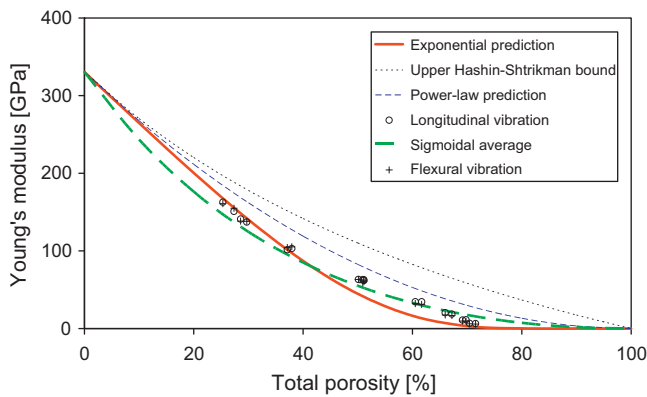


Fig. 18. Young's moduli of alumina–zirconia composites A60Z40 measured via the resonant frequency technique (circles) and the impulse excitation technique (pluses) and comparison with four admissible predictions (thin dotted – upper Hashin Shtrikman bound, thin dashed – power-law prediction, thick full – exponential prediction, thick dashed – sigmoidal average).

ues are compared with three types of predictions<sup>41,43–51</sup>: the Hashin–Shtrikman upper bound

$$E = E_0 \left( \frac{1 - \phi}{1 + \phi} \right), \quad (3)$$

the power-law relation

$$E = E_0(1 - \phi)^2, \quad (4)$$

the exponential relation

$$E = E_0 \exp \left( \frac{-2\phi}{1 - \phi} \right), \quad (5)$$

and the sigmoidal average

$$E = E_0 \left( \frac{(1 - \phi)^2}{1 + \phi} \right), \quad (6)$$

where  $\phi$  is the (total) porosity and  $E_0$  the Young's modulus of the solid phase, i.e. of the densely sintered matrix phase. The  $E_0$  values (corresponding to the Young's moduli of densely sin-

tered, pore-free alumina–zirconia composites) can be readily calculated when the materials are isotropic (our case) and the composition is known, because the Hashin–Shtrikman bounds are very tight in this case.<sup>41</sup> For the compositions of the present paper (A90Z10, A80Z20, A70Z30 and A60Z40) the  $E_0$  values are 383, 366, 349 and 331 GPa, respectively.<sup>41</sup> It is evident that all measured values (effective Young's moduli) for the porous composites are clearly below the upper Hashin–Shtrikman bound and also below the power-law prediction. However, both the exponential relation and the sigmoidal average provide a satisfactory prediction of the effective Young's modulus of alumina–zirconia composites with microstructures resulting from processing with pore-forming agents, with partial or complete sintering. We would like to emphasize, that the curves are parameter-free predictions, not fit curves. As such the results are remarkable, because – supported by previous findings for pure alumina, zirconia and ATZ composites<sup>22,52,53</sup> – they allow realistic estimates to be made for the elastic properties of porous ZTA composites with similar types of microstructure and thus to circumvent time-consuming measurements. More than this, they enhance confidence in the applicability of our exponential relation and the sigmoidal average for other materials as well. We note in passing that relations of the same type have been successfully applied also to other properties, e.g. thermal conductivity.<sup>21,51</sup> This supports our belief that these two relations (our exponential relation and the sigmoidal average) are of general validity in the sense that they are able to provide microstructure-dependent but material-independent predictions.

#### 4. Summary and conclusion

Alumina–zirconia composite ceramics with compositions on the alumina-rich side, so-called ZTA ceramics, have been prepared and characterized. Four compositions (with zirconia contents ranging 10, 20, 30 and 40 wt.%) and corn starch contents ranging from 10 to 50 vol.% (related to ceramic powders) have been prepared by starch consolidation casting, combined with partial or complete matrix sintering, and characterized by shrinkage, the Archimedes technique, image analysis and mercury porosimetry. Their Young's moduli have been measured via the resonant frequency technique and the impulse excitation technique.

It has been found that porosities of up to 70–71% can be achieved for partially sintered samples, while the highest porosities attainable with complete matrix sintering are only 50–51%. The pore cavity sizes (cell diameters) determined by image analysis (mean intercept technique) are 10–17  $\mu\text{m}$ , while mercury porosimetry yields information on the pore throat sizes (cell window diameters): these are monomodal after matrix sintering (1530 °C) with median diameter of approx. 1.4–2.2  $\mu\text{m}$ , but bimodal when the matrix is only partially sintered (1100–1400 °C), the second mode being at approx. 0.1–0.2  $\mu\text{m}$ . Thus the partially sintered materials have microstructure that can be described as hierarchical (with porosity at two levels). As expected, the microstructure of the porous ZTA composites is primarily determined by the processing route (e.g. the firing temperature), whereas the material composition

has a minor influence; however, a change in pore shape has been observed (from convex to concave with increasing zirconia content), which has a certain influence also on the measured pore size. The Young's moduli measured are remarkably close to our exponential relation (a theoretically well-founded effective-medium approximation) and the sigmoidal average. That means, for microstructures obtained by the processing method indicated (starch consolidation casting combined with partial or complete matrix sintering) it is possible – with the precision shown in the graphs – to predict the effective Young's moduli of porous alumina–zirconia composite ceramics without measuring.

## Acknowledgements

This study was part of the frame research programme MSM 6046137302 “Preparation and research of functional materials and material technologies using micro- and nanoscopic methods”, supported by the Ministry of Education, Youth and Sports of the Czech Republic. Support is gratefully acknowledged. The authors also thank Dipl.-Min. M. Keuper and Dr. C. Berthold from the Institute for Mineralogy and Geodynamics of the University Tübingen (Germany) for the great help with XRD and SEM.

## References

- Lee WE, Rainforth WM. *Ceramic microstructures—property control by processing*. London: Chapman & Hall; 1994. p. 534–8.
- Wachtman JB. *Mechanical properties of ceramics*. New York: John Wiley & Sons; 1996. p. 391–407.
- Becher PF, Rose LRF. Toughening mechanisms in ceramic systems. In: Swain M, vol. editor. Structure and properties of ceramics (=vol. 11 of Cahn RW, Haasen P, Kramer EJ. Materials science and technology—a comprehensive treatment), Wiley-VCH, Weinheim; 2005. p. 409–61.
- Gibson LJ, Ashby MF. *Cellular solids – structure and properties*. second edition Cambridge: Cambridge University Press; 1997. p. 93–344.
- Scheffler M, Colombo P, editors. *Cellular ceramics*. Weinheim: Wiley-VCH; 2005. p. 3–17, 225–400.
- Rice RW. *Porosity of ceramics*. New York: Marcel Dekker; 1998. p. 1–374.
- Corbin SF, Apte PS. Engineered porosity via tape casting, lamination and the percolation threshold of pyrolyzable particulates. *J Am Ceram Soc* 1999;**82**:1693–701.
- Davis J, Kristoffersson A, Carlström E, Clegg W. Fabrication and crack deflection in ceramic laminates with porous interlayers. *J Am Ceram Soc* 2000;**83**:2369–74.
- Galassi C, Roncari E, Capiani C, Fabbri G, Piancastelli A, Peselli M, et al. Processing of porous PZT materials for underwater acoustics. *Ferroelectrics* 2002;**268**:47–52.
- Kim JG, Sim JH, Cho WS. Preparation of porous (Ba, Sr)TiO<sub>3</sub> by adding corn-starch. *J Phys Chem Solids* 2002;**63**:2079–84.
- Díaz A, Hampshire S. Characterization of porous silicon nitride materials produced with starch. *J Eur Ceram Soc* 2004;**24**:413–9.
- Mattern A, Huchler B, Staudenecker D, Oberacker R, Nagel A, Hoffmann MJ. Preparation of interpenetrating ceramic-metal composites. *J Eur Ceram Soc* 2004;**24**:3399–408.
- Reynaud C, Thévenot F, Chartier T, Besson J-L. Mechanical properties and mechanical behaviour of SiC dense-porous laminates. *J Eur Ceram Soc* 2005;**25**:589–97.
- Barea R, Osendi MI, Ferreira JMF, Miranzo P. Thermal conductivity of highly porous mullite material. *Acta Mater* 2005;**53**:3313–8.
- Galassi C. Processing of porous ceramics—piezoelectric materials. *J Eur Ceram Soc* 2006;**26**:2951–8.
- García-Gabaldón M, Pérez-Herranz V, Sánchez E, Mestre S. Effect of porosity on the effective electrical conductivity of different ceramic membranes used as separators in electrochemical reactors. *J Membr Sci* 2006;**280**:536–44.
- Gregorová E, Pabst W, Boháčenko I. Characterization of different starch types for their application in ceramic processing. *J Eur Ceram Soc* 2006;**26**:1301–9.
- Gregorová E, Živcová Z, Pabst W. Porosity and pore space characteristics of starch-processed porous ceramics. *J Mater Sci* 2006;**41**:6119–22.
- Gregorová E, Živcová Z, Pabst W. Porous ceramics made using potato starch as a pore-forming agent. *Fruit Veg Cereal Sci Biotechnol* 2009;**3**:115–27.
- Gregorová E, Živcová Z, Pabst W. Starch as a pore-forming and body-forming agent in ceramic technology. *Starch/Stärke* 2009;**61**:495–502.
- Živcová Z, Gregorová E, Pabst W, Smith DS, Michot A, Poulier C. Thermal conductivity of porous alumina ceramics prepared using starch as a pore-forming agent. *J Eur Ceram Soc* 2009;**29**:347–53.
- Živcová Z, Černý M, Pabst W, Gregorová E. Elastic properties of porous oxide ceramics prepared using starch as a pore-forming agent. *J Eur Ceram Soc* 2009;**29**:2765–71.
- Gregorová E, Pabst W, Živcová Z, Sedlářová I, Holíková S. Porous alumina ceramics prepared with wheat flour. *J Eur Ceram Soc* 2010;**30**:2871–80.
- Lyckfeldt O, Ferreira JMF. Processing of porous ceramics by “starch consolidation”. *J Eur Ceram Soc* 1998;**18**:131–40.
- Alves HM, Tarí G, Fonseca AT, Ferreira JMF. Processing of porous cordierite bodies by starch consolidation. *Mater Res Bull* 1998;**33**:1439–48.
- Lemos AF, Ferreira JMF. Porous bioactive calcium carbonate implants processed by starch consolidation. *Mater Sci Eng* 2000;**C11**:35–40.
- Pabst W, Týnová E, Mikač J, Gregorová E, Havrda J. A model for the body formation in starch consolidation casting. *J Mater Sci Lett* 2002;**21**:1101–3.
- Týnová E, Pabst W, Gregorová E, Havrda J. Starch consolidation casting of alumina ceramics—body formation and microstructural characterization. *Key Eng Mater* 2002;**206–213**:1969–72.
- Bowden ME, Rippey MS. Porous ceramics formed using starch consolidation. *Key Eng Mater* 2002;**206–213**:1957–60.
- Týnová E, Pabst W, Mikač J. Starch swelling and its role in modern ceramic shaping technology. *Macromol Symp* 2003;**203**:295–300.
- Romano P, Velasco FJ, Torralba JM, Candela N. Processing of M2 powder metallurgy high-speed steel by means of starch consolidation. *Mater Sci Eng A* 2006;**419**:1–7.
- Gregorová E, Pabst W. Porosity and pore size control in starch consolidation casting—achievements and problems. *J Eur Ceram Soc* 2007;**27**:669–72.
- Mao X, Wang S, Shimai S. Porous ceramics with tri-modal pores prepared by foaming and starch consolidation. *Ceram Intern* 2008;**34**:107–12.
- Živcová Z, Gregorová E, Pabst W. Low- and high-temperature processes and mechanisms in the preparation of porous ceramics via starch consolidation casting. *Starch/Stärke* 2010;**62**:3–10.
- Rahaman MN. *Ceramic processing and sintering*. second edition New York: Marcel Dekker; 2003. p. 470–506.
- German RM. *Sintering theory and practice*. New York: John Wiley and Sons; 1996. p. 67–177.
- Saltykov SA. *Stereometrische metallurgie*. Leipzig: VEB Deutscher Verlag für Grundstoffindustrie; 1974. p. 87–128, 243–329 (in German).
- Hilliard JE, Lawson LR. *Stereology and stochastic geometry*. Dordrecht: Kluwer Academic Publishers; 2003. p. 125–277.
- Russ JC, Dehoff RT. *Practical stereology*. second edition New York: Kluwer Academic/Plenum Publishers; 2000. p. 1–77.
- Gregg SJ, Sing KSW. *Adsorption, surface area and porosity*. second edition London: Academic Press; 1982. p. 173–94.
- Pabst W, Gregorová E. Effective elastic moduli of alumina zirconia and alumina–zirconia composites. In: Caruta BM, editor. *Ceramics and composite materials*. New York: Nova Science Publishers; 2006. p. 31–100.
- Green DJ. *An Introduction to the mechanical properties of ceramics*. Cambridge: Cambridge University Press; 1998. p. 70–104.
- Pabst W, Gregorová E. Note on the so-called Coble–Kingery formula for the effective tensile modulus of porous ceramics. *J Mater Sci Lett* 2003;**22**:959–62.

44. Pabst W, Gregorová E. Derivation of the simplest exponential and power-law relations for the effective tensile modulus of porous ceramics via functional equations. *J Mater Sci Lett* 2003;**22**:1673–5.
45. Pabst W, Gregorová E. New relation for the porosity dependence of the effective tensile modulus of brittle materials. *J Mater Sci* 2004;**39**:3501–3.
46. Pabst W, Gregorová E. Effective elastic properties of alumina–zirconia composite ceramics—Part II: Micromechanical modeling. *Ceram Silik* 2004;**48**:14–23.
47. Pabst W, Gregorová E. Mooney-type relation for the porosity dependence of the effective tensile modulus of ceramics. *J Mater Sci* 2004;**39**:3213–5.
48. Pabst W, Gregorová E, Tichá G. Elasticity of porous ceramics—a critical study of modulus-porosity relations. *J Eur Ceram Soc* 2006;**26**:1085–97.
49. Pabst W, Gregorová E, Tichá G. Effective properties of suspensions, composites and porous materials. *J Eur Ceram Soc* 2007;**27**:479–82.
50. Pabst W, Gregorová E, Hostaša J. Phase mixture models for the thermal conductivity of nanofluids and nanocrystalline solids. *AIP Conf Proc* 2009;**1145**:109–12.
51. Pabst W, Gregorová E. *Phase mixture models for the properties of nanoceramics*. New York: Nova Science Publishers; 2010. p. 1–69.
52. Pabst W, Gregorová E, Tichá G, Týnová E. Effective elastic properties of alumina–zirconia composite ceramics—Part IV: tensile modulus of porous alumina and zirconia. *Ceram Silik* 2004;**48**:145–53.
53. Pabst W, Tichá G, Gregorová E, Týnová E. Effective elastic properties of alumina–zirconia composite ceramics—Part V: tensile modulus of alumina–zirconia composite ceramics. *Ceram Silik* 2005;**49**:77–85.
54. Minaříková M. Ceramic layers based on  $\text{Al}_2\text{O}_3\text{--ZrO}_2$ . M.Sc. thesis, ICT Prague; 2002 (in Czech).
55. Schreiber E, Anderson OL, Soga N. *Elastic constants and their measurement*. New York: McGraw-Hill; 1973. p. 82–125.
56. ASTM Standard C1259. Standard test method for dynamic Young's modulus, shear modulus, and Poisson's ratio for advanced ceramics by impulse excitation of vibration, ASTM International, West Conshohocken, PA, 2008, doi:10.1520/C1259-08E01, [www.astm.org](http://www.astm.org).
57. Pabst W, Gregorová E. Effective elastic properties of alumina–zirconia composite ceramics—Part I: rational continuum theory of linear elasticity. *Ceram Silik* 2003;**47**:1–7.
58. Slamovich EB, Lange FF. Densification of large pores (I—experimental). *J Am Ceram Soc* 1992;**75**:2498–508.